Article

Fast Radio Burst Energy Function in the Presence of DM_host Variation

Ji-Guo Zhang [1] , Yichao Li [1]*, Jia-Ming Zou [1], Ze-Wei Zhao [1], Jing-Fei Zhang [1] and Xin Zhang [1,2,3]*

1   Key Laboratory of Cosmology and Astrophysics (Liaoning Province) & Department of Physics, College of Sciences, Northeastern University, Shenyang 110819, China; zhangjiguo@stumail.neu.edu.cn (J.-G.Z.); neuxiao1@163.com (J.-M.Z.); zhaozw@stumail.neu.edu.cn (Z.-W.Z.); jfzhang@mail.neu.edu.cn (J.-F.Z.)
2   Key Laboratory of Data Analytics and Optimization for Smart Industry (Ministry of Education), Northeastern University, Shenyang 110819, China
3   National Frontiers Science Center for Industrial Intelligence and Systems Optimization, Northeastern University, Shenyang 110819, China
*   Correspondence: liyichao@mail.neu.edu.cn (Y.L.); zhangxin@mail.neu.edu.cn (X.Z.)

Abstract: Fast radio bursts (FRBs) have been found in great numbers, but the physical mechanism of these sources is still a mystery. The redshift evolutions of the FRB energy distribution function and the volumetric rate shed light on the origin of FRBs. However, such estimations rely on the dispersion measurement (DM)–redshift (z) relationship. A few FRBs that have been detected recently show large excess DMs beyond the expectation from the cosmological and Milky Way contributions, which indicates large spread of DMs from their host galaxies. In this work, we adopt two lognormal-distributed DM_{host} models and estimate the energy function using the non-repeating FRBs selected from the Canadian Hydrogen Intensity Mapping Experiment (CHIME)/FRB Catalog 1. By comparing the lognormal-distributed DM_{host} models to a constant DM_{host} model, the FRB energy function results are consistent within the measurement uncertainty. We also estimate the volumetric rate of the non-repeating FRBs in three different redshift bins. The volumetric rate shows that the trend is consistent with the stellar-mass density redshift evolution. Since the lognormal-distributed DM_{host} model increases the measurement errors, the inference of FRBs tracking the stellar-mass density is nonetheless undermined.

Keywords: fast radio bursts; redshift; energy function; event rates

1. Introduction

Fast radio bursts (FRBs) are bright, violent flashes of radio emission with durations in the order of milliseconds. In 2007, the first FRB event was discovered by Lorimer et al. [1] from the archived data of the Parkes telescope in Australia. In 2013, four FRB events were discovered by the Green Bank Telescope (GBT) [2]. In 2017, Chatterjee et al. [3] for the first time confirmed the host galaxy of one FRB, i.e., FRB 20121102A, which was discovered by the Arecibo radio telescope [4]. At this point, ∼800 FRB sources have been discovered, with frequencies from hundreds of MHz to several GHz, by advanced radio telescopes [1], such as the Canadian Hydrogen Intensity Mapping Experiment (CHIME) [2] and the Australian Square Kilometre Array Pathfinder (ASKAP) [3], etc. Most of the FRBs are non-repeating events, and dozens of sources are repeaters emitting repeating bursts (see ref. [5] for a comprehensive review).

There is still an open question of the origin of FRBs (see ref. [6] for a recent review). A series of theoretical models have been proposed to elucidate how FRBs originate [7]. Typically, FRBs can come from strange quark stars. This idea is supported by the ∼16-day periodicity of FRB 20180916B, which can be explained by the collapse of the crust of a strange quark star [8]. Accurate localizations of FRBs within their individual hosts also give us hints about their origin. In 2020, the galactic magnetar SGR J1935+2154 [9,10] was found to produce an FRB that coincided in time with a non-thermal X-ray burst from the magnetar. This supports the conjecture that some FRBs may be produced by magnetars. The repeating FRB 20200120E, localized at the position of a globular cluster in M81 [11], suggests an old

stellar population as the progenitor. This is because globular clusters are usually composed of old stars with low metal content. By contrast, the repeating FRB 20201124A was localized to a massive, star-forming galaxy [12] at a redshift of $z = 0.098$ [13]. There is no consensus in determining the type of FRB hosts. Nevertheless, the redshift of an FRB can be inferred from its unique host galaxy, which enables valuable cosmological applications as the localized FRBs accumulate in great numbers [14–23]; see refs. [24,25] for recent reviews. For more information on FRB hosts, refer to the comprehensive catalog of the 23 localized FRBs with secure hosts provided by ref. [26]. The limited number of localized events to date, however, hinders our ability to fully understand the origin of FRBs.

The FRB energy function [27–29] is also an effective way to constrain the origin models of FRBs. The energy functions allow us to study the redshift evolution of the volumetric rate of FRBs. To achieve this, the intensity distribution function can also be studied [30]. If FRBs originate from young stellar populations, the volumetric FRB rate should rise with increasing redshift as the density of the cosmic star formation rate increases towards a higher redshift (up to $z \sim 2$). Conversely, if FRB progenitors are old, such as white dwarfs, neutron stars, or black holes, the volumetric rate should follow the evolution of stellar mass, which is barely evolved at low redshift. Ref. [31] found no significant redshift evolution in the number density of non-repeating FRB sources, which is consistent with the stellar-mass evolution in the universe. In their recent research, ref. [32] reported that old progenitors like neutron stars and black holes are more likely to be the progenitors of non-repeating FRBs.

Recently, a few FRBs have shown larger excess DMs than what is typically expected from the cosmological and Milky Way contributions [3,4,33–35]. In particular, Niu et al. [36] reported the detection of FRB 190520B with $DM_{host} \approx 903^{+72}_{-111} \, pc \, cm^{-3}$, which is almost an order of magnitude higher than the average DM_{host} of the FRBs discovered so far. The uncertainties from DM_{host} can inevitably skew the inferred redshifts of unlocalized FRBs when employing the DM–z relationship for estimation [37,38], which poses challenges to revealing their underlying engine and potential use as cosmological probes. Therefore, it is crucial to investigate the impact of DM_{host} uncertainty on the redshift inference of FRBs and the associated population properties. In this work, we study the effect of DM_{host} uncertainty on the FRB energy function estimation as well as the redshift evolution of the FRB event rate. Note that in this work, the *Planck* 2018 Λ cold dark matter model is adopted as a fiducial model, with the best-fit cosmological parameters $H_0 = 67.36 \, km \, s^{-1} \, Mpc^{-1}$, $\Omega_b = 0.0493$, $\Omega_m = 0.3153$, and $\Omega_\Lambda = 0.6847$.

This paper is organized as follows: In Section 2, we describe the FRB catalog as well as the selection criteria used in this work. The Bayesian framework used for the redshift estimation is described in Section 3. In Section 4, we present the energy functions and volumetric rates of non-repeating FRB sources along with their redshift evolution. The conclusions are presented in Section 5.

2. Data

2.1. FRB Catalog

We use the first release of the CHIME/FRB catalog [10], which contains 474 non-repeating bursts and 62 repeating bursts from 18 repeaters. The 536 burst events were detected from 2018 July 25 to 2019 July 1 over an effective survey duration of 214.8 days. In order to minimize the selection effects, a number of criteria are suggested [32,39].

1. Events with `bonsai_snr`< 10 are rejected, where `bonsai_snr` is the signal-to-noise ratio (S/N) recorded in the catalog. Ref. [39] suggests a S/N cut of 12 since the signal below S/N = 12 may be misclassified as radio-frequency interference (RFI). In this work, we use bursts with S/Ns over 10, which maintains a meaningful number of FRB samples for the statistical analysis [32].
2. Events with $DM_{obs} < 1.5 \times max(DM_{NE2001}, DM_{YMW16})$ are rejected to ensure the extragalactic origin of the events. DM_{obs} is the measured DM; DM_{NE2001} and DM_{YMW16}

are the DMs of the Milky Way estimated according to the NE2001 model [40] and the YMW16 model [41], respectively.

3. Events with $\lg(\tau_{scat}/ms) > 0.8$ are rejected, where τ_{scat} is the scattering timescale. Note that lg is equivalent to $\log_{10}$ in this work.

4. Events with $\lg(F_\nu/Jy\,ms) < 0.5$ are rejected, where F_ν is the fluence of the burst.

5. Events detected in the side lobes of the telescope's primary beam are rejected.

After applying the selection criteria, we have 176 FRB events selected, including 12 repeaters.

Previous analysis with mock data indicated that a significant fraction of FRBs were missed by the CHIME detection algorithm, i.e., only 39,638 out of 84,697 injected mock events were detected [39]. The total number of events (N_{FRB}) needs to be scaled from the observed number of events (N_{obs}) according to the detection fraction:

$$N_{FRB} = N_{obs} \times \frac{84,697}{39,638}. \tag{1}$$

In addition, the fraction of missed events also depends on the properties of the FRB signals. Longer scattering times or lower fluencies result in a higher number of missed events. Following ref. [10], the relationship between the observed and intrinsic data distributions is described by

$$P(\vartheta) = P_{obs}(\vartheta) \times s(\vartheta)^{-1}, \tag{2}$$

where $P(\vartheta)$ and $P_{obs}(\vartheta)$ represent the intrinsic and observed distributions of the FRB property ϑ, respectively. The symbol $s(\vartheta)$ is the selection function as a function of different FRB properties. The properties considered for deriving the selection function include the dispersion measure (DM_{obs}), scattering timescale (τ_{scat}), intrinsic duration (w_{int}), and fluence (F_ν); see ref. [10] for details. We adopt the best-fit selection functions in ref. [32]:

$$s(\widehat{DM}_{obs}) = -0.7707 \left(\lg \widehat{DM}_{obs} \right)^2 + 4.5601 \left(\lg \widehat{DM}_{obs} \right) - 5.6291, \tag{3}$$

$$s(\widehat{\tau}_{scat}) = -0.2922 \left(\lg \widehat{\tau}_{scat} \right)^2 - 1.0196 \left(\lg \widehat{\tau}_{scat} \right) + 1.4592, \tag{4}$$

$$s(\widehat{w}_{int}) = -0.0785 \left(\lg \widehat{w}_{int} \right)^2 - 0.5435 \left(\lg \widehat{w}_{int} \right) + 0.9574, \tag{5}$$

$$\lg s(\widehat{F}_\nu) = 1.7173 \left(1 - \exp \left(-2.0348 \lg \widehat{F}_\nu \right) \right) - 1.7173, \tag{6}$$

where $\widehat{DM}_{obs} = \left(\frac{DM_{obs}}{pc\,cm^{-3}} \right)$, $\widehat{\tau}_{scat} = \left(\frac{\tau_{scat}}{ms} \right)$, $\widehat{w}_{int} = \left(\frac{w_{int}}{ms} \right)$, and $\widehat{F}_\nu = \left(\frac{F_\nu}{Jy\,ms} \right)$.

2.2. Galaxy Catalog

In order to evaluate the redshifts of the unlocalized FRBs, we follow the method developed in ref. [42], which actually employs the dark siren method in gravitational wave cosmology [43–45]. It assumes that an FRB is always located in a galaxy and that the redshift of the FRB can be statistically estimated by associating the FRB event with its potential host galaxies according to an underlying galaxy catalog.

In this work, we adopt the galaxy catalog from Dark Energy Spectroscopic Instrument (DESI) Legacy Surveys. The Legacy Surveys combine three imaging projects of different telescopes, i.e., the Beijing–Arizona Sky Survey (BASS) [46], the Dark Energy Camera Legacy Survey (DECaLS) [47], and the Mayall z-band Legacy Survey (MzLS) [48], covering about $14000\,deg^2$ of the northern hemisphere and producing the target catalog for the DESI survey; for an overview of the Legacy Surveys, see ref. [49]. We use the galaxy sample from the eighth public data release of the Legacy Surveys, i.e., Data Release 8 (DR8) [50]. The spectroscopic redshift of the galaxy sample is substituted for the photometric redshift, if available, in accordance with the sample selection process in ref. [51]. In total, the

galaxy sample incorporates 129.35 million galaxies, among which 2.1 million galaxies have spectroscopic redshifts. The redshift distribution of the DR8 galaxies is shown in Figure 1. Finally, 145 one-off FRBs are selected, as they reside within the region covered by the galaxy catalog, and their sky locations are shown in Figure 2 with the black circles. The footprint of the galaxy sample is illustrated with the red area, where the galaxies residing in the south galactic cap (SGCP) and the north galactic cap (NGCP) are shown in the left and right panels, respectively.
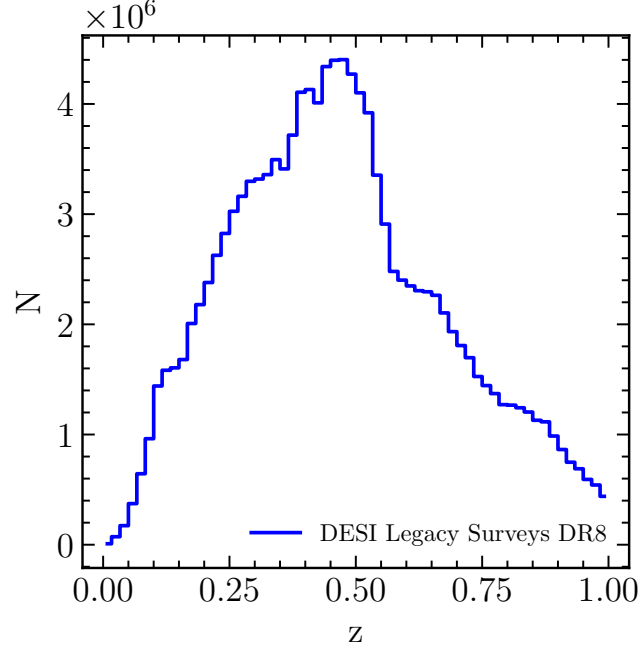

Figure 1. The redshift distribution of DESI Legacy Surveys DR8 galaxy catalog.
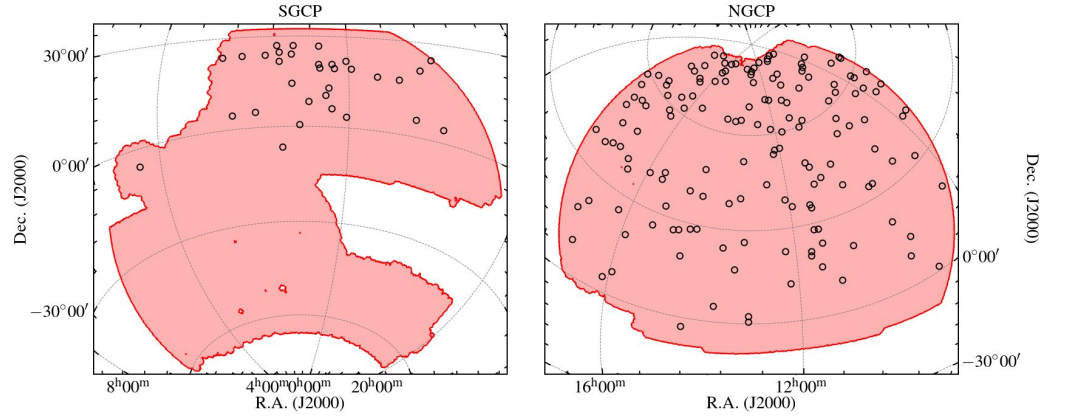

Figure 2. The sky locations of 145 selected FRB sources (one-off FRBs) within the region covered by the DR8 galaxies. The FRBs are shown with the black circles, and the footprint of the galaxy sample used in this work is shown with the red area. The galaxies within the SGCP and the NGCP are shown in the left and right panels, respectively.

3. Methods

3.1. Bayesian Framework

We adopt a Bayesian data analysis scheme to measure the FRBs' redshifts. The Bayesian inference relates the probability density functions (PDFs) involving data and parameters:

$$P(\vartheta|x) \propto P(\vartheta)P(x|\vartheta), \tag{7}$$

where $P(x|\vartheta)$ is the likelihood function of the data given the model parameters, and $P(\vartheta|x)$ is the posterior PDF, i.e., the PDF of the parameters given the data set. In this work, we shall estimate the posterior PDF of the FRBs' redshifts z given the measurement set of DM:

$$P(z|\text{DM}) \propto P(z)P(\text{DM}|z), \tag{8}$$

where $P(\text{DM}|z)$ represents the likelihood function of the measured DM given the parameter set. The measured DM is the combination of several components:

$$\text{DM} = \text{DM}_{\text{MW}} + \text{DM}_{\text{halo}} + \text{DM}_{\text{IGM}} + \frac{\text{DM}_{\text{host}}}{1+z}, \tag{9}$$

where the contributions are from the interstellar medium of the Milky Way (DM_{MW}), the ionized gas in the local halo (DM_{halo}), the intergalactic medium (DM_{IGM}), and the FRB host galaxy (DM_{host}).

The variable DM_{MW} can be subtracted according to the current models. The CHIME/FRB catalog provides the dispersion measure with the Milky Way contribution subtracted using the NE2001 [40] or YMW16 models [41]. We test both of the models and find no significant difference in the final estimation. In the following analysis, only the results with the YMW16 model are presented.

The precise contribution of the local halo to DMs is uncertain. Ref. [52] provides the prediction of DM_{halo} with a mean value of $43\,\text{pc}\,\text{cm}^{-3}$ and a full range of $30\text{–}245\,\text{pc}\,\text{cm}^{-3}$. We adopt the mean value of $43\,\text{pc}\,\text{cm}^{-3}$ in the following analysis.

After subtracting DM_{MW} and DM_{halo} for the total DM, the measurement likelihood function is written as

$$P(\text{DM}|z) = \int \mathrm{d}\,\text{DM}_{\text{host}}\,\mathrm{d}\,\text{DM}_{\text{IGM}}\,P(\text{DM}|\text{DM}_{\text{host}}, \text{DM}_{\text{IGM}}, z)$$
$$\times\ P(\text{DM}_{\text{host}}|z)P(\text{DM}_{\text{IGM}}|z), \tag{10}$$

where $P(\text{DM}_{\text{host}}|z)$ and $P(\text{DM}_{\text{IGM}}|z)$ are the likelihood functions of DM_{host} and DM_{IGM}, respectively, and the integration represents the marginalization of the DM_{host} and DM_{IGM} likelihood function.

3.2. $P(\text{DM}_{\text{IGM}}|z)$

The DM contribution from the IGM (DM_{IGM}) can be explained as the dispersion induced when an FRB is emitted at a random point in the universe of redshift z and propagates to $z = 0$. The average value of DM_{IGM} at redshift z is given by the integration of the free electron number density n_{e} along the line of sight:

$$\langle \text{DM}_{\text{IGM}} \rangle = \int_0^z \mathrm{d}z' \frac{n_{\text{e}}(z')}{1+z'} \left(\frac{1}{1+z'} \frac{c}{H_0} \frac{1}{E(z')} \right), \tag{11}$$

In this work, we consider the standard flat ΛCDM model $E(z) = \sqrt{\Omega_{\text{m}}(1+z)^3 + \Omega_{\Lambda}}$. Assuming the universe is fully ionized at $z \lesssim 3$, the free electron number density equals the total electron number density:

$$n_{\text{e}}(z) = f_{\text{IGM}}\bar{\rho}_{\text{b},0}(1+z)^3 \left(\frac{Y_{\text{H}}\chi_{\text{e,H}}(z)}{m_{\text{p}}} + 2\frac{Y_{\text{He}}\chi_{\text{e,He}}(z)}{4m_{\text{p}}} \right), \tag{12}$$

where $Y_{\text{H}} \sim 3/4$ and $Y_{\text{He}} \sim 1/4$ denote the primordial mass fractions of hydrogen and helium, respectively. The ionization fractions $\chi_{\text{e,H}}(z)$ and $\chi_{\text{e,He}}(z)$ for hydrogen and helium are both set to unity at the redshift of $z \lesssim 3$ [53,54]. The symbol $\bar{\rho}_{\text{b},0} = 3H_0^2\Omega_{\text{b}}/8\pi G$ is the comoving cosmological baryon density at the current epoch, m_{p} is the mass of a proton, and $f_{\text{IGM}} \approx 0.83$ represents the fraction of the free electrons in the IGM [55].

The DM_{IGM} deviation from $\langle DM_{IGM} \rangle$ is expected to follow the normal distribution. Thus, the likelihood function is expressed as

$$P(DM_{IGM}|z) = \frac{1}{\mathcal{N}_{IGM}} \exp\left(-\frac{1}{2} \frac{(DM_{IGM} - \langle DM_{IGM} \rangle)^2}{\sigma_{IGM}^2} \right), \tag{13}$$

where $\mathcal{N}_{IGM} = \sigma_{IGM}\sqrt{2\pi}$ is the normalization factor, and σ_{IGM} is fitted in a power-law form [56]:

$$\sigma_{IGM} = 173.8 \, z^{0.4} \text{ pc cm}^{-3}. \tag{14}$$

3.3. $P(DM_{host}|z)$

The major uncertainty of the FRB redshift measurement comes from the variation of the DM contribution from the FRB's host galaxy. A few FRBs show large excess DMs beyond the expectation from the the cosmological and Milky Way contributions [3,4,33,34]. Recently, Niu et al. [36] reported the detection of FRB 190520B with $DM_{host} \approx 903^{+72}_{-111}$ pc cm^{-3}, which is almost an order of magnitude higher than the average DM_{host} of the FRBs discovered so far. Broadly speaking, the large spread of the DM_{host} can be modeled using a lognormal distribution, and the corresponding likelihood function is expressed as

$$P(DM_{host}|z) = \frac{1}{\mathcal{N}_{host}} \exp\left(-\frac{1}{2} \frac{(\ln x - \mu)^2}{\sigma_{host}^2} \right), \tag{15}$$

where $x = DM_{host}/\text{pc cm}^{-3}$, $\mathcal{N}_{host} = x\sigma_{host}\sqrt{2\pi}$ is the normalization factor, and μ and σ_{host} are both the lognormal distribution parameters. Using a cosmological magnetohydrodynamical simulation, Mo et al. [57] proposed a detailed analysis of the distribution of DM_{host} for various FRB population models. In this work, we adopt the fitting result of

$$\mu = \ln(63.55), \; \sigma_{host} = 1.25 \tag{16}$$

from Mo et al. [57] (hereafter referred to as the Mo22 model). In addition, Zhang et al. [58] (hereafter referred to as the Zhang20 model) provided another fitting result:

$$\mu = \ln\left(32.97(1+z)^{0.84} \right), \; \sigma_{host} = 1.248. \tag{17}$$

We compare the differences in results obtained using such two DM_{host} distribution models (expressed in Equations (16) and (17)), as well as use the model of assuming a constant $DM_{host} = 50$ pc cm^{-3}.

3.4. The Posterior Distribution of the FRB Redshifts

The DM measurement likelihood function is expressed as

$$P(DM|DM_{host}, DM_{IGM}, z) = \frac{1}{\mathcal{N}} \exp\left(-\frac{1}{2} \frac{(DM - \Theta)^2}{\sigma_{DM}^2} \right), \tag{18}$$

where $\mathcal{N} = \sigma_{DM}\sqrt{2\pi}$ is the normalization factor, σ_{DM} is the measurement uncertainty, and $\Theta = DM_{host} + DM_{IGM} + DM_{MW} + DM_{halo}$ represents the DM's theoretical value. Substituting Equations (13), (15), and (18) into Equation (10), we can estimate the posterior probability at a given redshift. Assuming the FRBs are always located in the galaxies, we shall use the redshifts of the galaxy catalog, i.e., the DESI Legacy Surveys DR8 galaxy catalog, as the prior distribution. For a given FRB, we utilize the redshifts of the selected galaxies in the DR8 catalog with their celestial coordinates α (right ascension) and δ (declination) satisfying the following criteria:

$$|\alpha_{gal} - \alpha_{FRB}| < \theta_\alpha \times \cos(\delta_{FRB}), \; |\delta_{gal} - \delta_{FRB}| < \theta_\delta, \tag{19}$$

where α_{gal} and δ_{gal} are the coordinates of the galaxies, while α_{FRB} and δ_{FRB} are the coordinates of the FRB. θ_α and θ_δ are the 68% confidence pointing errors of the CHIME beam in the right ascension and declination directions, respectively. The estimated redshift posterior probabilities are shown in Figure 3. For each FRB event, the posterior probability is estimated at the redshift of each potential host galaxy, which is selected from the DESI Legacy Surveys DR8 galaxies sample residing in the sky area determined by Equation (19). The colors indicate the value of $DM_{IGM} + DM_{host}$ of the FRB event. There is a clear trend of FRBs with larger DMs having their posterior probability distribution peaking at higher redshifts, which is consistent with the Macquart relation [59]. However, the posterior probability also shows a wide range of distribution, indicating the large uncertainty of the redshift estimation. Such large uncertainty is primarily due to the large scattering of DM_{IGM} (see Equation (14)). Additionally, the prior distribution of the galaxy catalog from DESI Legacy Surveys DR8 introduces uncertainty, particularly at high redshifts, where the photometric redshifts of galaxies are less accurate.
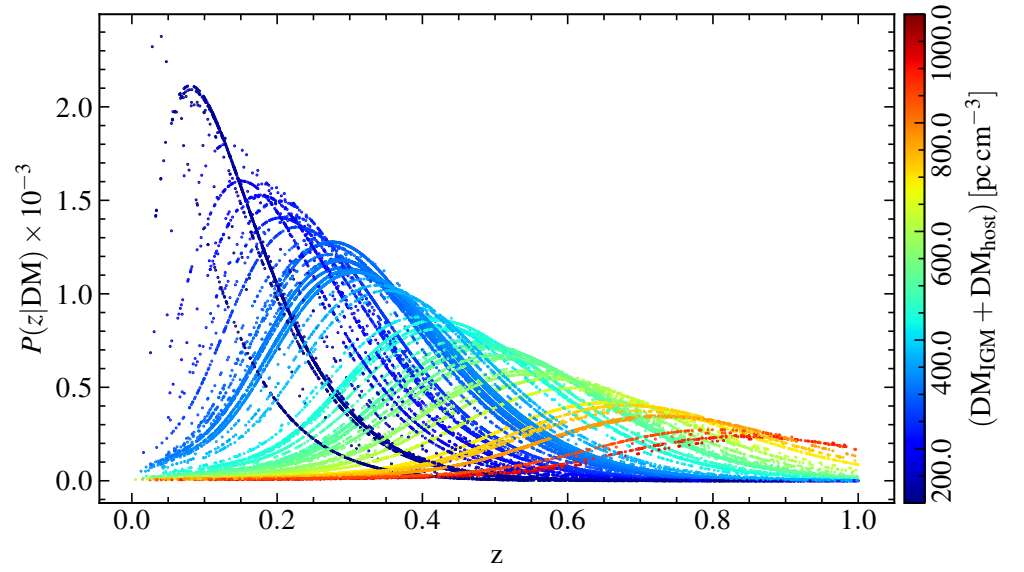

Figure 3. The redshift posterior probability distribution of each FRB event. Each curve represents the posterior probability of one FRB using the DESI Legacy Surveys DR8 galaxy redshift sample that located in the sky area determined by Equation (19). The colors of the lines indicate the values of $DM_{IGM} + DM_{host}$.

3.5. Energy Function

The FRB fluence (F_ν) is converted to rest-frame isotropic radio energy (E) for each FRB via [60]:

$$E = \frac{4\pi d_L^2}{(1+z)^{2+\alpha_F}} F_\nu \Delta\nu, \qquad (20)$$

where d_L is the luminosity distance to the FRB, α_F is the spectrum index of the FRB's power-law spectrum across frequencies (note that α_F differs from α_{FRB} in Equation (19)), and $\Delta\nu$ is the burst bandwidth. The burst bandwidth is calculated by `high_freq−low_freq` in the CHIME/FRB Catalog 1, where `high_freq` and `low_freq` represent the upper and lower bands, respectively, of the detection at full-width tenth-maximum (FWTM) [10]. The spectrum index term, $(1+z)^{-\alpha_F}$, represents the bandwidth k-correction since the event emitted its radiation in a different band than that in which it was observed. It is known that there are narrow-band FRBs, such as the repeating FRB 20201124A discussed in Zhou et al. [61], and the spectrum index for the non-power-law spectrum is tricky to define. The CHIME/FRB Catalog 1 provided the spectrum index for both the broad- and narrow-band FRBs but used an additional spectrum-running parameter, reshaping the spectra to match different bandwidths. As long as the k-correction is negligible for the narrow-band

spectrum, Equation (20) is available for both broad- and narrow-band FRBs. In addition, the narrow-band FRBs are mostly repeating FRBs [62]. This work focuses on the non-repeating FRBs, which are mostly broad-band ones. We assume a constant power-law index and take $\alpha_F = -1.5$ from CHIME/FRB Collaboration et al. [10].

The FRB energy function represents the number density of FRB events as a function of energy. To estimate this function, we adopt the V_{max} method [63,64], which defines V_{max} as the flux-limited maximum volume within which the FRB event could still be detected [63,64]:

$$V_{max} = \frac{4\pi}{3}\left(\chi_{max}^3 - \chi_{min}^3\right),$$ (21)

where χ_{min} and χ_{max} are the comoving distances at the minimum and maximum redshifts, respectively. We adopt $z_{min} = 0.05$ in this work, and z_{max} is estimated according to the fluence of the FRB:

$$F_\nu = \frac{E(1 + z_{max})^{2 + \alpha_F}}{4\pi d_{L, z_{max}}^2 \Delta \nu} > 10^{0.5} \text{ Jy ms}.$$ (22)

The number density for a single FRB event is defined as the inverse of V_{max}, and the number density per unit of time is expressed as

$$\rho_{obs} = \frac{1}{V_{max} f_{sky}(t_{obs}/(1 + z))},$$ (23)

where $f_{sky} = 3 \times 10^{-3}$ is the fraction of the sky covered by the CHIME's field of view, $t_{obs} = 0.59$ yr is the survey time for the CHIME/FRB Catalog 1, and the factor of $1 + z$ converts the survey time to the rest frame. Furthermore, ρ_{obs} needs to be corrected for the selection effect, as mentioned in Section 2.1. Considering the selection function of Equations (3)–(6), the corrected number density is [32]

$$\rho_{corr} = \frac{1}{\mathcal{N}_s} W \rho_{obs},$$ (24)

where $W = \left(s(DM_{obs})s(\tau_{scat})s(w_{int})s(F_\nu)\right)^{-1}$. $\mathcal{N}_s = \sum_i W_i / N_{FRB}$ is the normalization factor, where i denotes the i-th FRB event, and N_{FRB} is the corrected total number defined in Equation (1).

We divide the full energy range occupied by the FRB detection into a number of energy bins in the logarithmic scale and sum ρ_{corr} within each energy bin; then, the FRB energy function is

$$\phi_j = \frac{1}{\Delta_j \lg E} \sum_i \rho_{corr,i},$$ (25)

where $\Delta_j \lg E$ is the j-th energy bin size.

We perform a Monte Carlo (MC) simulation with 10000 realizations of the redshift sample following the posterior probability distribution of Equation (10). The energy function is estimated using each of the realizations. The uncertainty is evaluated via the the standard deviation.

4. Results and Discussion

Figure 4 shows the energy functions estimated using the CHIME/FRB Catalog 1. The energy functions are estimated within three redshift bins, i.e., $0.05 < z \leqslant 0.30$, $0.30 < z \leqslant 0.68$, and $0.68 < z \leqslant 1.38$ (following ref. [32]). The estimated energy distribution functions of different redshift bins are shown in different colors. The results with different DM_{host} models, i.e., the Mo22 model and the Zhang20 model, are shown in the upper and bottom panels of Figure 4, respectively.
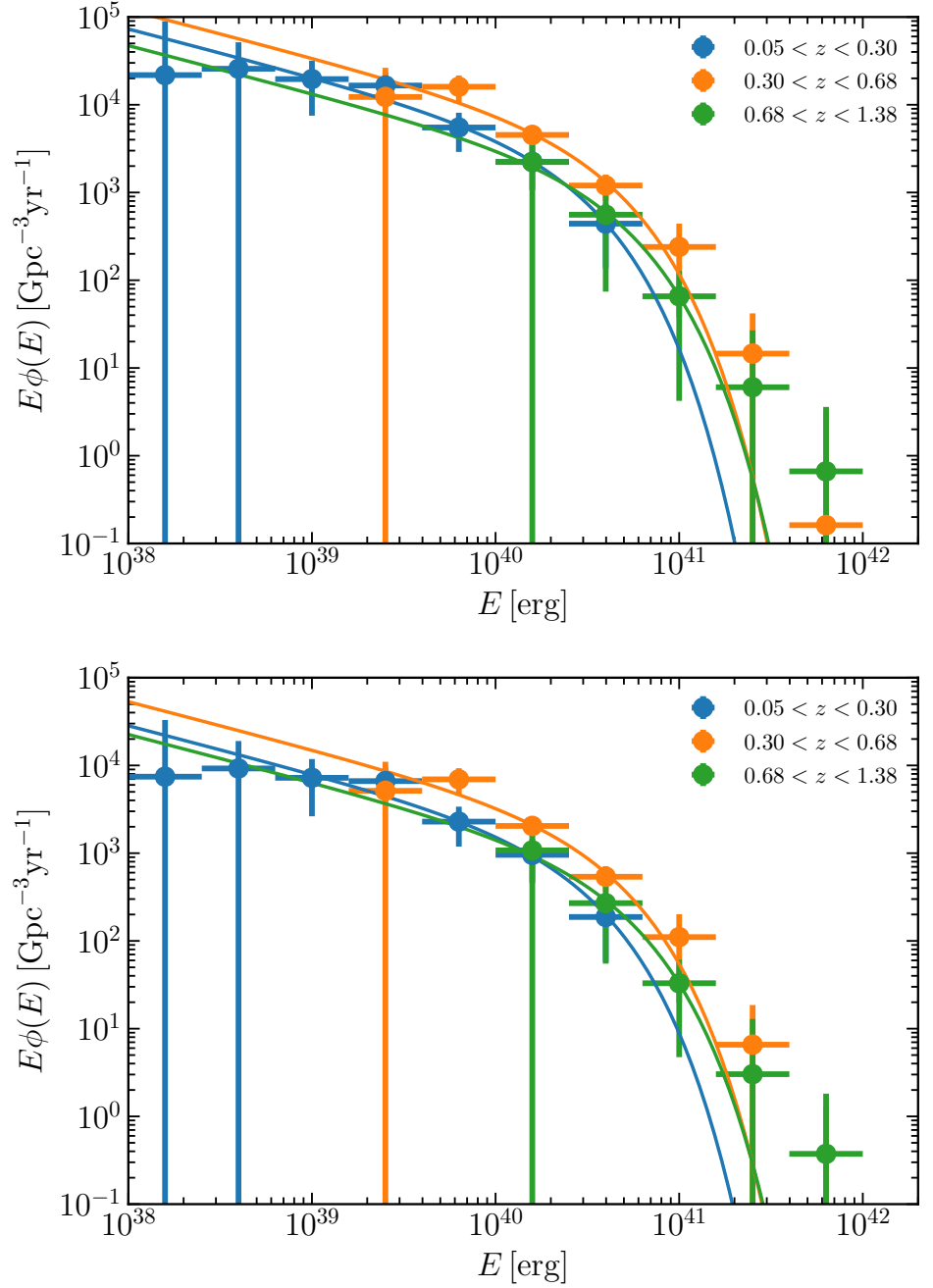
Figure 4. The energy functions of non-repeating CHIME FRB sources using the Mo22 model (upper panel) and the Zhang20 model (bottom panel). In each panel, the results for three redshift bins are shown with three different colors, and the best-fit Schechter functions are shown with solid lines.

The FRB energy distribution is modeled with a Schechter function [65]:

$$\phi(\lg E)\,\mathrm{d}\lg E = \phi^{\star}\left(\frac{E}{E^{\star}}\right)^{\gamma+1}\exp\left(-\frac{E}{E^{\star}}\right)\mathrm{d}\lg E, \tag{26}$$

where $\phi^{\star}$ is the normalization factor, $\gamma+1$ is the faint-end slope, and $E^{\star}$ is the break energy of the Schechter function. The energy distribution functions are fitted to the measurements using the public package emcee [4] [66]. We use $\phi^{\star}$, $E^{\star}$, and γ as free parameters for the first redshift bin, i.e., $0.05 < z \leqslant 0.30$. Due to the lack of FRB data in the higher redshift bins, we

only use $\phi^\star$ and $E^\star$ as the free parameters in the remaining two redshift bins and fix γ to the best-fit values of the first redshift bin.

The best-fit energy distribution functions at each redshift bin are shown with the smooth curves in Figure 4. The energy functions estimated in each redshift bin are mutually consistent. There is no significant redshift evolution for using either the Mo22 model or the Zhang20 model. The best-fit values of parameters in Equation (26) are listed in Table 1. The volumetric rate of the FRBs (Φ_{FRB}) is estimated by integrating the energy function within the energy range available for each redshift bin, which spans 10^{37}–10^{43} erg s^{-1} according to ref. [28].
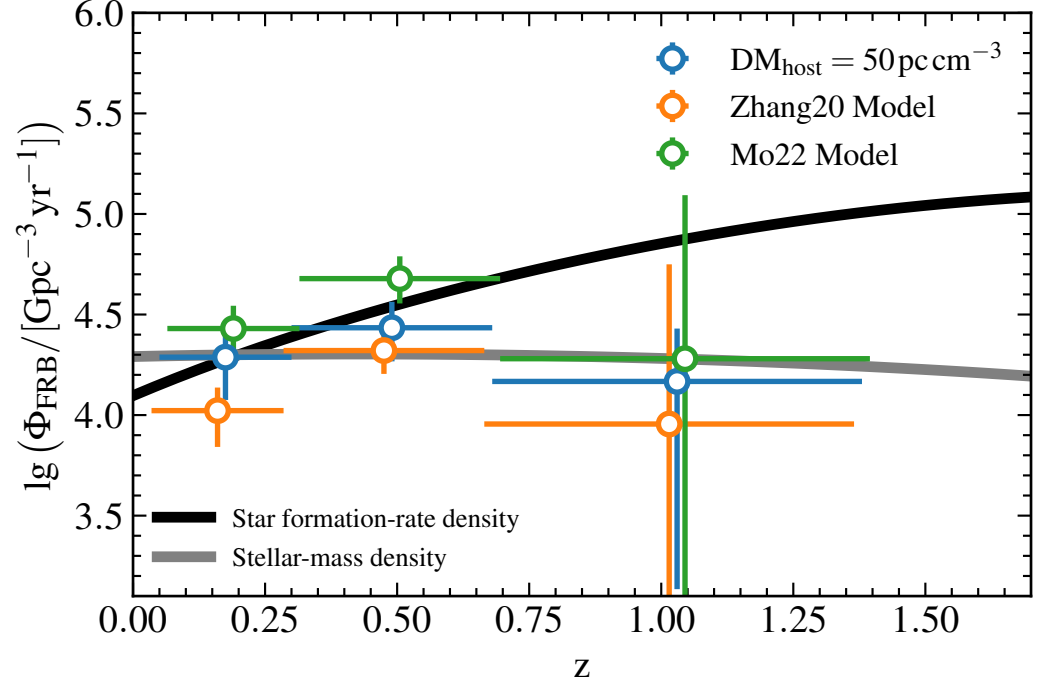

Figure 5. The volumetric rate of CHIME non-repeating FRBs as a function of redshift. The horizontal errors represent the redshift bin width, and the vertical errors indicate the estimation uncertainty; estimates are based on 10000 iterations of the MC simulation. The results from the constant $\mathrm{DM}_{\mathrm{host}}$ model, the Zhang20 model, and the Mo22 model are shown with different colors. The solid black and gray curves show the cases of the star formation rate and the stellar-mass density, respectively, which are both estimated using the fitting functions in ref. [31].

The corresponding volumetric rates estimated using the best-fit energy functions are listed in the last column of Table 1 and are also shown in Figure 5. The figure illustrates the FRB volumetric rates for different $\mathrm{DM}_{\mathrm{host}}$ models. It also includes solid lines of the star formation rate and the stellar-mass density, each estimated using the fitting functions in ref. [31]. Both of the curves are normalized for their amplitudes at redshift $z = 0.2$ to the same value as the FRB volumetric rates estimated using the constant $\mathrm{DM}_{\mathrm{host}}$.

With the constant $\mathrm{DM}_{\mathrm{host}}$ assumption, the FRB volumetric rate shows the same trend as the stellar-mass density, which is consistent with the previous analysis [32]. By releasing the constant $\mathrm{DM}_{\mathrm{host}}$ assumption, the uncertainty increases, especially for the high redshift bin. Within the estimated error, there is no significant difference between using and not using the constant $\mathrm{DM}_{\mathrm{host}}$ assumption. However, it can be seen that the variation of $\mathrm{DM}_{\mathrm{host}}$ weakens the conclusion that the volumetric rate is consistent with the case of stellar-mass density. It is expected that future, much larger FRB and galaxy samples could greatly improve the measurement and help draw a more solid conclusion.

Table 1. The best-fit parameters (i.e., $\phi^\star$, $E^\star$, and γ) in the Schechter function for the FRB energy function using the CHIME/FRB Catalog 1 with different redshift bins and DM_{host} models, and the estimated volumetric rates of the FRBs (Φ_{FRB}) are shown in the last column. Here, E^* is in units of erg, while ϕ^* and Φ_{FRB} are both in units of $Gpc^{-3}\,yr^{-1}$.

	$\lg E^\star$	$\lg \phi^\star$	γ	$\lg \Phi_{FRB}$
	$0.05 < z \leqslant 0.30$			
Constant DM_{host}	$40.000^{+0.428}_{-0.363}$	$3.994^{+0.254}_{-0.626}$	$-1.046^{+0.516}_{-0.373}$	$4.277^{+0.139}_{-0.301}$
Zhang20 Model	$40.219^{+0.592}_{-0.378}$	$3.418^{+0.358}_{-0.877}$	$-1.382^{+0.572}_{-0.224}$	$4.035^{+0.125}_{-0.192}$
Mo22 Model	$40.225^{+0.589}_{-0.382}$	$3.783^{+0.369}_{-0.882}$	$-1.427^{+0.537}_{-0.238}$	$4.438^{+0.121}_{-0.181}$
	$0.30 < z \leqslant 0.68$			
Constant DM_{host}	$40.239^{+0.169}_{-0.119}$	$4.097^{+0.164}_{-0.222}$	–	$4.434^{+0.129}_{-0.167}$
Zhang20 Model	$40.503^{+0.177}_{-0.150}$	$3.370^{+0.207}_{-0.226}$	–	$4.321^{+0.113}_{-0.116}$
Mo22 Model	$40.496^{+0.183}_{-0.153}$	$3.729^{+0.211}_{-0.235}$	–	$4.678^{+0.111}_{-0.123}$
	$0.68 < z \leqslant 1.38$			
Constant DM_{host}	$40.408^{+0.216}_{-0.451}$	$3.772^{+0.336}_{-0.847}$	–	$4.167^{+0.263}_{-1.033}$
Zhang20 Model	$40.553^{+0.461}_{-1.549}$	$2.970^{+1.640}_{-0.470}$	–	$3.956^{+0.794}_{-1.869}$
Mo22 Model	$40.547^{+0.534}_{-1.519}$	$3.295^{+2.204}_{-0.003}$	–	$4.280^{+0.813}_{-1.992}$

5. Conclusions

In this work, we estimate the energy function and the volumetric rate of the non-repeating FRBs using the CHIME/FRB Catalog 1. We follow the FRB selection criteria as used in refs. [32,39]. In the meantime, we follow the Bayesian framework data analysis scheme developed in ref. [42] and adopt the galaxy catalog from DESI Legacy Surveys to estimate redshifts of the unlocalized FRBs.

We also consider different DM_{host} models, including a constant-DM_{host} model of assuming $DM_{host} = 50\,pc\,cm^{-3}$ as well as a couple of lognormal distribution models: namely, the Mo22 model and the Zhang20 model. The FRB energy function is estimated with each of the DM_{host} models.

The Schechter-function-like energy function model is considered and fitted to the measurements using the non-repeating FRBs from the CHIME/FRB Catalog 1. We do not find a significant difference between using the constant DM_{host} model and the two lognormal DM_{host} models (i.e., the Mo22 model and the Zhang20 model).

We also estimate the FRB volumetric rates according to the best-fit energy distribution function and compare the trends of redshift evolution with the star formation rate density and the stellar-mass density. We find that with the lognormal DM_{host} models, the uncertainties increase. The trend of redshift evolution is consistent with the stellar-mass density for the constant DM_{host} model and the lognormal DM_{host} models. However, since the lognormal-distributed DM_{host} model increases the measurement errors, the inference of FRBs tracking the stellar-mass density is nonetheless undermined. The measurement can be further improved in the future by using a larger FRB catalog and/or a deeper galaxy survey catalog.

Author Contributions: Conceptualization, Y.L. and X.Z.; methodology, J.-G.Z.; software, Y.L. and J.-G.Z.; validation, J.-G.Z and J.-M.Z.; formal analysis, J.-F.Z.; investigation, Z.-W.Z.; writing—original draft preparation, Y.L.; writing—review and editing, J.-G.Z; supervision, J.-F.Z. and X.Z.; project administration, X.Z. All authors have read and agreed to the published version of the manuscript.

Institutional Review Board Statement: Not applicable.

Informed Consent Statement: Not applicable.

Data Availability Statement: The code that supports this work is publicly available at https://github.com/YichaoLi/frb_efunc (accessed on 5 May 2024).

Conflicts of Interest: The authors declare no conflicts of interest.

Notes

1   https://blinkverse.alkaidos.cn, accessed on 5 May 2024
2   https://www.chime-frb.ca/catalog, accessed on 5 May 2024
3   https://www.atnf.csiro.au/projects/askap/index.html, accessed on 5 May 2024
4   https://emcee.readthedocs.io/en/stable/index.html, accessed on 5 May 2024

References

1.   Lorimer, D.R.; Bailes, M.; McLaughlin, M.A.; Narkevic, D.J.; Crawford, F. A Bright Millisecond Radio Burst of Extragalactic Origin. *Science* **2007**, *318*, 777. https://doi.org/10.1126/science.1147532.
2.   Thornton, D.; Stappers, B.; Bailes, M.; Barsdell, B.; Bates, S.; Bhat, N.D.R.; Burgay, M.; Burke-Spolaor, S.; Champion, D.J.; Coster, P.; et al. A Population of Fast Radio Bursts at Cosmological Distances. *Science* **2013**, *341*, 53–56. https://doi.org/10.1126/science.1236789.
3.   Chatterjee, S.; Law, C.J.; Wharton, R.S.; Burke-Spolaor, S.; Hessels, J.W.T.; Bower, G.C.; Cordes, J.M.; Tendulkar, S.P.; Bassa, C.G.; Demorest, P.; et al. The direct localization of a fast radio burst and its host. *Nature* **2017**, *541*, 58. https://doi.org/10.1038/nature20797.
4.   Spitler, L.G.; Cordes, J.M.; Hessels, J.W.T.; Lorimer, D.R.; McLaughlin, M.A.; Chatterjee, S.; Crawford, F.; Deneva, J.S.; Kaspi, V.M.; Wharton, R.S.; et al. Fast Radio Burst Discovered in the Arecibo Pulsar ALFA Survey. *Astrophys. J.* **2014**, *790*, 101. https://doi.org/10.1088/0004-637X/790/2/101.
5.   Hu, C.R.; Huang, Y.F. A Comprehensive Analysis of Repeating Fast Radio Bursts. *Astrophys. J. Suppl.* **2023**, *269*, 17. https://doi.org/10.3847/1538-4365/acf566.
6.   Zhang, B. Solving the Mystery of Fast Radio Bursts: A Detective's Approach. *Universe* **2023**, *9*, 375. https://doi.org/10.3390/universe9080375.
7.   Platts, E.; Weltman, A.; Walters, A.; Tendulkar, S.P.; Gordin, J.E.B.; Kandhai, S. A Living Theory Catalogue for Fast Radio Bursts. *Phys. Rept.* **2019**, *821*, 1–27. https://doi.org/10.1016/j.physrep.2019.06.003.
8.   Geng, J.; Li, B.; Huang, Y. Repeating fast radio bursts from collapses of the crust of a strange star. *Innovation* **2021**, *2*, 100152. https://doi.org/10.1016/j.xinn.2021.100152.
9.   Bochenek, C.D.; Ravi, V.; Belov, K.V.; Hallinan, G.; Kocz, J.; Kulkarni, S.R.; McKenna, D.L. A fast radio burst associated with a Galactic magnetar. *Nature* **2020**, *587*, 59–62. https://doi.org/10.1038/s41586-020-2872-x.
10.   CHIME/FRB Collaboration.; Amiri, M.; et al. The First CHIME/FRB Fast Radio Burst Catalog. *Astrophys. J. Suppl.* **2021**, *257*, 59, https://doi.org/10.3847/1538-4365/ac33ab.
11.   Bhardwaj, M.; Gaensler, B.M.; Kaspi, V.M.; Landecker, T.L.; Mckinven, R.; Michilli, D.; Pleunis, Z.; Tendulkar, S.P.; Andersen, B.C.; Boyle, P.J.; et al. A Nearby Repeating Fast Radio Burst in the Direction of M81. *Astrophys. J. Lett.* **2021**, *910*, L18. https://doi.org/10.3847/2041-8213/abeaa6.
12.   Fong, W.; Dong, Y.; Leja, J.; Bhandari, S.; Day, C.K.; Deller, A.T.; Kumar, P.; Prochaska, J.X.; Scott, D.R.; Bannister, K.W.; et al. Chronicling the Host Galaxy Properties of the Remarkable Repeating FRB 20201124A. *Astrophys. J. Lett.* **2021**, *919*, L23. https://doi.org/10.3847/2041-8213/ac242b.
13.   Nimmo, K.; Hewitt, D.M.; Hessels, J.W.T.; Kirsten, F.; Marcote, B.; Bach, U.; Blaauw, R.; Burgay, M.; Corongiu, A.; Feiler, R.; et al. Milliarcsecond Localization of the Repeating FRB 20201124A. *Astrophys. J. Lett.* **2022**, *927*, L3. https://doi.org/10.3847/2041-8213/ac540f.
14.   Gao, H.; Li, Z.; Zhang, B. Fast Radio Burst/Gamma-Ray Burst Cosmography. *Astrophys. J.* **2014**, *788*, 189. https://doi.org/10.1088/0004-637X/788/2/189.

15. Zhou, B.; Li, X.; Wang, T.; Fan, Y.Z.; Wei, D.M. Fast radio bursts as a cosmic probe? *Phys. Rev. D* **2014**, *89*, 107303. https://doi.org/10.1103/PhysRevD.89.107303.

16. Zhao, Z.W.; Li, Z.X.; Qi, J.Z.; Gao, H.; Zhang, J.F.; Zhang, X. Cosmological parameter estimation for dynamical dark energy models with future fast radio burst observations. *Astrophys. J.* **2020**, *903*, 83. https://doi.org/10.3847/1538-4357/abb8ce.

17. Qiu, X.W.; Zhao, Z.W.; Wang, L.F.; Zhang, J.F.; Zhang, X. A forecast of using fast radio burst observations to constrain holographic dark energy. *JCAP* **2022**, *2*, 6. https://doi.org/10.1088/1475-7516/2022/02/006.

18. Wu, P.J.; Shao, Y.; Jin, S.J.; Zhang, X. A path to precision cosmology: Synergy between four promising late-universe cosmological probes. *JCAP* **2023**, *6*, 52. https://doi.org/10.1088/1475-7516/2023/06/052.

19. Zhao, Z.W.; Wang, L.F.; Zhang, J.G.; Zhang, J.F.; Zhang, X. Probing the interaction between dark energy and dark matter with future fast radio burst observations. *JCAP* **2023**, *4*, 22. https://doi.org/10.1088/1475-7516/2023/04/022.

20. Yang, K.B.; Wu, Q.; Wang, F.Y. Finding the Missing Baryons in the Intergalactic Medium with Localized Fast Radio Bursts. *Astrophys. J. Lett.* **2022**, *940*, L29. https://doi.org/10.3847/2041-8213/aca145.

21. Wang, B.; Wei, J.J. An 8.0% Determination of the Baryon Fraction in the Intergalactic Medium from Localized Fast Radio Bursts. *Astrophys. J.* **2023**, *944*, 50. https://doi.org/10.3847/1538-4357/acb2c8.

22. Zhang, J.G.; Zhao, Z.W.; Li, Y.; Zhang, J.F.; Li, D.; Zhang, X. Cosmology with fast radio bursts in the era of SKA. *Sci. China Phys. Mech. Astron.* **2023**, *66*, 120412. https://doi.org/10.1007/s11433-023-2212-9.

23. Wei, J.J.; Melia, F. Investigating Cosmological Models and the Hubble Tension Using Localized Fast Radio Bursts. *Astrophys. J.* **2023**, *955*, 101. https://doi.org/10.3847/1538-4357/acefb8.

24. Bhandari, S.; Flynn, C. Probing the Universe with Fast Radio Bursts. *Universe* **2021**, *7*, 85. https://doi.org/10.3390/universe7040085.

25. Xiao, D.; Wang, F.; Dai, Z. The physics of fast radio bursts. *Sci. China Phys. Mech. Astron.* **2021**, *64*, 249501. https://doi.org/10.1007/s11433-020-1661-7.

26. Gordon, A.C.; fai Fong, W.; Kilpatrick, C.D.; Eftekhari, T.; Leja, J.; Prochaska, J.X.; Nugent, A.E.; Bhandari, S.; Blanchard, P.K.; Caleb, M.; et al. The Demographics, Stellar Populations, and Star Formation Histories of Fast Radio Burst Host Galaxies: Implications for the Progenitors. *Astrophys. J.* **2023**, *954*, 80. https://doi.org/10.3847/1538-4357/ace5aa.

27. Zhang, R.C.; Zhang, B.; Li, Y.; Lorimer, D.R. On the energy and redshift distributions of fast radio bursts. *Mon. Not. Roy. Astron. Soc.* **2021**, *501*, 157–167. https://doi.org/10.1093/mnras/staa3537.

28. Luo, R.; Men, Y.; Lee, K.; Wang, W.; Lorimer, D.R.; Zhang, B. On the FRB luminosity function – – II. Event rate density. *Mon. Not. Roy. Astron. Soc.* **2020**, *494*, 665–679. https://doi.org/10.1093/mnras/staa704.

29. James, C.W.; Prochaska, J.X.; Macquart, J.P.; North-Hickey, F.O.; Bannister, K.W.; Dunning, A. The fast radio burst population evolves, consistent with the star formation rate. *Mon. Not. Roy. Astron. Soc.* **2022**, *510*, L18–L23. https://doi.org/10.1093/mnrasl/slab117.

30. Li, L.; Huang, Y.; Zhang, Z.; Li, D.; Li, B. Intensity Distribution Function and Statistical Properties of Fast Radio Bursts. *Res. Astron. Astrophys.* **2017**, *17*, 6. https://doi.org/10.1088/1674-4527/17/1/6.

31. Hashimoto, T.; Goto, T.; On, A.Y.L.; Lu, T.Y.; Santos, D.J.D.; Ho, S.C.C.; Kim, S.J.; Wang, T.W.; Hsiao, T.Y.Y. No redshift evolution of non-repeating fast radio-burst rates. *Mon. Not. Roy. Astron. Soc.* **2020**, *498*, 3927–3945. https://doi.org/10.1093/mnras/staa2490.

32. Hashimoto, T.; Goto, T.; On, A.Y.L.; Lu, T.Y.; Santos, D.J.D.; Ho, S.C.C.; Kim, S.J.; Wang, T.W.; Hsiao, T.Y.Y. Energy functions of fast radio bursts derived from the first CHIME/FRB catalogue. *Mon. Not. Roy. Astron. Soc.* **2022**, *511*, 1961–1976. https://doi.org/10.1093/mnras/stac065.

33. Hardy, L.K.; Dhillon, V.S.; Spitler, L.G.; Littlefair, S.P.; Ashley, R.P.; De Cia, A.; Green, M.J.; Jaroenjittichai, P.; Keane, E.F.; Kerry, P.; et al. A search for optical bursts from the repeating fast radio burst FRB 121102. *Mon. Not. Roy. Astron. Soc.* **2017**, *472*, 2800–2807. https://doi.org/10.1093/mnras/stx2153.

34. Tendulkar, S.P.; Bassa, C.G.; Cordes, J.M.; Bower, G.C.; Law, C.J.; Chatterjee, S.; Adams, E.A.K.; Bogdanov, S.; Burke-Spolaor, S.; Butler, B.J.; et al. The Host Galaxy and Redshift of the Repeating Fast Radio Burst FRB 121102. *Astrophys. J. Lett.* **2017**, *834*, L7. https://doi.org/10.3847/2041-8213/834/2/L7.

35. Chittidi, J.S.; Simha, S.; Mannings, A.; Prochaska, J.X.; Ryder, S.D.; Rafelski, M.; Neeleman, M.; Macquart, J.P.; Tejos, N.; Jorgenson, R.A.; et al. Dissecting the Local Environment of FRB 190608 in the Spiral Arm of its Host Galaxy. *Astrophys. J.* **2021**, *922*, 173. https://doi.org/10.3847/1538-4357/ac2818.

36. Niu, C.H.; Aggarwal, K.; Li, D.; et al. A repeating fast radio burst associated with a persistent radio source. *Nature* **2022**, *606*, 873–877. https://doi.org/10.1038/s41586-022-04755-5.

37. Walker, C.R.H.; Ma, Y.Z.; Breton, R.P. Constraining the redshifts of unlocalised fast radio bursts. *Astron. Astrophys.* **2020**, *638*, A37. https://doi.org/10.1051/0004-6361/201833157.

38. James, C.W.; Ghosh, E.M.; Prochaska, J.X.; Bannister, K.W.; Bhandari, S.; Day, C.K.; Deller, A.T.; Glowacki, M.; Gordon, A.C.; Heintz, K.E.; et al. A measurement of Hubble's Constant using Fast Radio Bursts. *Mon. Not. Roy. Astron. Soc.* **2022**, *516*, 4862–4881. https://doi.org/10.1093/mnras/stac2524.

39. Shin, K.; Masui, K.W.; Bhardwaj, M.; Cassanelli, T.; Chawla, P.; Dobbs, M.; Dong, F.A.; Fonseca, E.; Gaensler, B.M.; Herrera-Martín, A.; et al. Inferring the Energy and Distance Distributions of Fast Radio Bursts Using the First CHIME/FRB Catalog. *Astrophys. J.* **2023**, *944*, 105. https://doi.org/10.3847/1538-4357/acaf06.

40. Cordes, J.M.; Lazio, T.J.W. NE2001.I. A New Model for the Galactic Distribution of Free Electrons and its Fluctuations. *arXiv* **2003**, http://arxiv.org/abs/astro-ph/0207156

41. Yao, J.M.; Manchester, R.N.; Wang, N. A new Electron-density Model for Estimation of Pulsar and frb Distances. *Astrophys. J.* **2017**, *835*, 29. https://doi.org/10.3847/1538-4357/835/1/29.

42. Zhao, Z.W.; Zhang, J.G.; Li, Y.; Zhang, J.F.; Zhang, X. FRB dark sirens: Measuring the Hubble constant with unlocalized fast radio bursts. *arXiv* **2024**. http://arxiv.org/abs/2212.13433.

43. Del Pozzo, W. Inference of the cosmological parameters from gravitational waves: application to second generation interferometers. *Phys. Rev. D* **2012**, *86*, 043011. https://doi.org/10.1103/PhysRevD.86.043011.

44. Wang, L.F.; Shao, Y.; Zhang, J.F.; Zhang, X. Ultra-low-frequency gravitational waves from individual supermassive black hole binaries as standard sirens. *arXiv* **2023**. http://arxiv.org/abs/2201.00607.

45. Song, J.Y.; Wang, L.F.; Li, Y.; Zhao, Z.W.; Zhang, J.F.; Zhao, W.; Zhang, X. Synergy between CSST galaxy survey and gravitational-wave observation: Inferring the Hubble constant from dark standard sirens. *Sci. China Phys. Mech. Astron.* **2024**, *67*, 230411. https://doi.org/10.1007/s11433-023-2260-2.

46. Zou, H.; Zhou, X.; Fan, X.; Zhang, T.; Zhou, Z.; Nie, J.; Peng, X.; McGreer, I.; Jiang, L.; Dey, A.; et al. Project Overview of the Beijing–Arizona Sky Survey. *Publ. Astron. Soc. Pac.* **2017**, *129*, 064101. https://doi.org/10.1088/1538-3873/aa65ba.

47. Flaugher, B.; Diehl, H.T.; Honscheid, K.; Abbott, T.M.C.; Alvarez, O.; Angstadt, R.; Annis, J.T.; Antonik, M.; Ballester, O.; Beaufore, L.; et al. The Dark Energy Camera. *Astron. J.* **2015**, *150*, 150. https://doi.org/10.1088/0004-6256/150/5/150.

48. Silva, D.R.; Blum, R.D.; Allen, L.; Dey, A.; Schlegel, D.J.; Lang, D.; Moustakas, J.; Meisner, A.M.; Valdes, F.; Patej, A.; et al. The Mayall z-band Legacy Survey. In *American Astronomical Society Meeting Abstracts #228*; American Astronomical Society Meeting Abstracts; American Astronomical Society: Washington, DC, USA, 2016; Volume 228, p. 317.02.

49. Dey, A.; Schlegel, D.J.; Lang, D.; Blum, R.; Burleigh, K.; Fan, X.; Findlay, J.R.; Finkbeiner, D.; Herrera, D.; Juneau, S.; et al. Overview of the DESI Legacy Imaging Surveys. *Astron. J.* **2019**, *157*, 168. https://doi.org/10.3847/1538-3881/ab089d.

50. Aihara, H.; Prieto, C.A.; An, D.; Anderson, S.F.; Éric Aubourg.; Balbinot, E.; Beers, T.C.; Berlind, A.A.; Bickerton, S.J.; Bizyaev, D.; et al. The Eighth Data Release of the Sloan Digital Sky Survey: First Data from SDSS-III. *Astrophys. J. Suppl.* **2011**, *193*, 29. https://doi.org/10.1088/0067-0049/193/2/29.

51. Yang, X.; Xu, H.; He, M.; Gu, Y.; Katsianis, A.; Meng, J.; Shi, F.; Zou, H.; Zhang, Y.; Liu, C.; et al. An Extended Halo-based Group/Cluster finder: Application to the DESI legacy imaging surveys DR8. *Astrophys. J.* **2021**, *909*, 143. https://doi.org/10.3847/1538-4357/abddb2.

52. Yamasaki, S.; Totani, T. The Galactic Halo Contribution to the Dispersion Measure of Extragalactic Fast Radio Bursts. *Astrophys. J.* **2020**, *888*, 105. https://doi.org/10.3847/1538-4357/ab58c4.

53. Fan, X.H.; Carilli, C.L.; Keating, B.G. Observational constraints on cosmic reionization. *Ann. Rev. Astron. Astrophys.* **2006**, *44*, 415–462. https://doi.org/10.1146/annurev.astro.44.051905.092514.

54. McQuinn, M.; Lidz, A.; Zaldarriaga, M.; Hernquist, L.; Hopkins, P.F.; Dutta, S.; Faucher-Giguere, C.A. HeII Reionization and its Effect on the IGM. *Astrophys. J.* **2009**, *694*, 842–866. https://doi.org/10.1088/0004-637X/694/2/842.

55. Deng, W.; Zhang, B. Cosmological Implications of Fast Radio Burst/Gamma-Ray Burst Associations. *Astrophys. J. Lett.* **2014**, *783*, L35. https://doi.org/10.1088/2041-8205/783/2/L35.

56. Qiang, D.C.; Wei, H. Effect of Redshift Distributions of Fast Radio Bursts on Cosmological Constraints. *Phys. Rev. D* **2021**, *103*, 083536. https://doi.org/10.1103/PhysRevD.103.083536.

57. Mo, J.F.; Zhu, W.; Wang, Y.; Tang, L.; Feng, L.L. The dispersion measure of Fast Radio Bursts host galaxies: estimation from cosmological simulations. *Mon. Not. Roy. Astron. Soc.* **2022**, *518*, 539–561. https://doi.org/10.1093/mnras/stac3104.

58. Zhang, G.Q.; Yu, H.; He, J.H.; Wang, F.Y. Dispersion measures of fast radio burst host galaxies derived from IllustrisTNG simulation. *Astrophys. J.* **2020**, *900*, 170. https://doi.org/10.3847/1538-4357/abaa4a.

59. Macquart, J.P.; Prochaska, J.; McQuinn, M.; et al. A census of baryons in the Universe from localized fast radio bursts. *Nature* **2020**, *581*, 391–395. https://doi.org/10.1038/s41586-020-2300-2.

60. Macquart, J.P.; Ekers, R. FRB event rate counts – II. Fluence, redshift, and dispersion measure distributions. *Mon. Not. Roy. Astron. Soc.* **2018**, *480*, 4211–4230. https://doi.org/10.1093/mnras/sty2083.

61. Zhou, D.J.; Han, J.L.; Zhang, B.; Lee, K.J.; Zhu, W.W.; Li, D.; Jing, W.C.; Wang, W.Y.; Zhang, Y.K.; Jiang, J.C.; et al. FAST Observations of an Extremely Active Episode of FRB 20201124A: I. Burst Morphology. *Res. Astron. Astrophys.* **2022**, *22*, 124001. https://doi.org/10.1088/1674-4527/ac98f8.

62. Pleunis, Z.; Good, D.C.; Kaspi, V.M.; Mckinven, R.; Ransom, S.M.; Scholz, P.; Bandura, K.; Bhardwaj, M.; Boyle, P.J.; Brar, C.; et al. Fast Radio Burst Morphology in the First CHIME/FRB Catalog. *Astrophys. J.* **2021**, *923*, 1. https://doi.org/10.3847/1538-4357/ac33ac.

63. Schmidt, M. Space Distribution and Luminosity Functions of Quasi-Stellar Radio Sources. *Astrophys. J.* **1968**, *151*, 393. https://doi.org/10.1086/149446.

64. Avni, Y.; Bahcall, J. On the simultaneous analysis of several complete samples-The V/Vmax and Ve/Va variables, with applications to quasars. *Astrophys. J.* **1980**, *235*, 694–716. https://doi.org/10.1086/157673.

65. Schechter, P. An analytic expression for the luminosity function for galaxies. *Astrophys. J.* **1976**, *203*, 297–306. https://doi.org/10.1086/154079.

66. Foreman-Mackey, D.; Hogg, D.W.; Lang, D.; Goodman, J. emcee: The MCMC Hammer. *Publ. Astron. Soc. Pac.* **2013**, *125*, 306–312. https://doi.org/10.1086/670067.